Biochemical and Biophysical Research Communications 373 (2008) 125–129

Contents lists available at ScienceDirect

Biochemical and Biophysical Research Communications

journal homepage: www.elsevier.com/locate/ybbrc

Tracking sperm in three-dimensions

G. Corkidi [a,*], B. Taboada [b], C.D. Wood [c], A. Guerrero [c], A. Darszon [c]

[a] Unidad de Microscopía Avanzada, Laboratorio de Imágenes y Visión por Computadora, Instituto de Biotecnología, Universidad Nacional Autónoma de México (UNAM), Apdo. Postal 510-3, Cuernavaca, 62250 Morelos, Mexico
[b] Centro de Ciencias Aplicadas y Desarrollo Tecnológico, Universidad Nacional Autónoma de México (UNAM), Apdo. Postal 70-186, Mexico, 04510 D.F., Mexico
[c] Departamento de Genética del Desarrollo y Fisiología Celular, Instituto de Biotecnología, Universidad Nacional Autónoma de México (UNAM), Apdo. Postal 510-3, Cuernavaca, 62250 Morelos, Mexico

ARTICLE INFO

Article history:
Received 27 May 2008
Available online 12 June 2008

Keywords:
Sperm tracking
Three-dimensional analysis
Motility

ABSTRACT

Sperm motility, crucial for fertilization, has been mostly studied in two dimensions (2D) by recording their swimming trajectories near a flat surface. However, spermatozoa swim in three-dimensions (3D) to find eggs, with their speed being the main impediment to track them under realistic conditions. Here, we describe a novel method allowing 3D tracking and analysis of the trajectories of multiple free-swimming sperm. The system uses a piezo-electric device displacing a large focal distance objective mounted on a microscope to acquire 70 image stacks per second, each stack composed of 60 images that span a depth of 100 μm. With this method, 3D paths of multiple sperm in the same field could be visualized simultaneously during 1 s . Within the same sample we found that surface-confined sperm swam 25% slower, produced 3-fold fewer circular revolutions per second, and had trajectories of 134% greater radius of curvature than those sperm swimming freely in 3D.

The fundamental task of spermatozoa, a highly specialized cell, is to deliver its genetic material to the female egg of its species. Inherently, this function requires for sperm to be motile. Tracking sperm in 3D, as they naturally swim, is an ambitious endeavour. The main obstacle to recording trajectories in 3D is the high speed with which these flagellated cells move (30–200 μM/s, [1,2]). While the qualitative 3D helical movement of sperm was observed long ago [3], Hiramoto and Baba. [4] compared quantitatively for the first time the speed and diameter of 2D sperm paths when focusing the microscope at two different levels (near a flat surface, and 300 μm distant from any boundary layer). Later, Crenshaw [5] reported the first system capable of tracking 3D trajectories of single sea urchin spermatozoa for quantitative analysis. He adapted a technology to track, in 3D, low-speed single microorganisms keeping them focused at the center of the microscope field that was developed by Berg [6], but which is not directly applicable to high speed motile cells, such as spermatozoa. The system proposed by Crenshaw comprised two video cameras that were attached to two perpendicularly-orientated microscopes (one camera giving the *X*, Y coordinates and the other one the *X*, Z coordinates). Focusing the microscopes to the center of a volume, images were recorded and analyzed frame by frame to determine the screen coordinates. Qualitative 3D trajectories were presented in this work in which exposure to an attractant stimulated sperm swimming. Quantitative parameters such as speed, curvature, and torsion were also presented as an example for a single sperm [7]. The mathematical theory of helical motion and chemotaxis with simulated microorganisms has been explored in further studies [8–13].

Here, we present a new image acquisition approach for 3D multi-tracking of spermatozoa using a single camera and a single microscope. A piezoelectric device was mounted between a long working distance objective of a microscope and the turret. This device was excited with an amplified triangular signal to generate vertical displacements in the objective at up to 70 cycles per second, while acquiring synchronously at successive focal planes (in a depth of 100 μm) the images of free-swimming spermatozoa at a rate of 4200 images per second. This produced the necessary data for reconstructing their trajectories in 3D.

To prove the usefulness of the proposed system, we present comparative results of the mean speed, mean radius of curvature, and the average number of revolutions/s of a sea urchin spermatozoa population when swimming freely in a three-dimensional sea water volume and when swimming circularly in 2D over the surface of a Petri dish. Sea urchin sperm were chosen as they naturally convert to a stable two dimensional trajectory when encountering a surface [14].

Materials and methods

Biological preparation. Sperm were obtained 'dry' from the sea urchin *Strongylocentrotrus purpuratus* (Marinus Inc., Long Beach,

* Corresponding author. Fax: +52 777 3291710.
E-mail addresses: corkidi@sgima.ceingebi.unam.mx, corkidi@ibt.unam.mx (G. Corkidi).

0006-291X/$ - see front matter © 2008 Elsevier Inc. All rights reserved.
doi:10.1016/j.bbrc.2008.05.189

CA, USA; Pamanes S. A. de C.V., Ensenada, Mexico) by intracoelomic injection of 0.5 M KCl and stored on ice. Artificial sea water (ASW) contained (mM): 430 NaCl, 10 KCl, 10 $CaCl_2$, 23 $MgCl_2$, 25 $MgSO_4$, 2 $NaHCO_3$, and 1 EDTA (pH 8.0, 950–1000 mosM). Petri dishes used as imaging chambers were briefly immersed into a 0.1% (wt/vol) solution of polyHEME in ethanol, hot-air blow-dried to rapidly evaporate the solvent. Dry sperm were diluted 1/10 in modified ASW (low Ca^{2+} (1 mM) pH 7.0), thereafter a 2 μl aliquot was further diluted $\sim 2.5 \times 10^5$ volumes in ASW and transferred to the imaging chamber.

The equipment. A schematic representation of the system setup is presented in Fig. 1. A piezoelectric device P-725 (Physik Instruments, MA, USA) was mounted between a 40× 0.55 NA long working distance objective (Nikon Ph 2 DL) and the inverted microscope (Nikon Eclipse TE2000-U). This piezoelectric device was controlled by a servo-controller E-501 via a high current amplifier E-505 (Physik Instruments, MA, USA). The servo-controller was excited with a triangular signal from a 3311A function generator (Hewlett Packard, CA, USA). A synchronizing signal coming from the servo-controller was used for triggering the high speed camera Motion-Pro HS4 (Redlake, AZ, USA) with 4 GB RAM (for recording up to 2 s or 8400 images of 512×512 pixels). The microscope was mounted on a heavy metal plate which had an inflated inner tube resting on a heavy marble table to isolate the system from external vibrations. The imaging chamber containing the biological preparation was mounted in an external support inserted between the microscope objective and the condenser to isolate it from the vibrations produced by the piezoelectric device. The temperature of the biological preparation was measured with a BAT-10R multi-purpose ±0.1° rechargeable thermometer, using a BT-1 general purpose thermocouple probe (Physitemp Instruments, NJ, USA). *X*,*Y* calibration was achieved using a calibrated glass slide (stage micrometer) with a 1 mm ruler having 10 μm divisions. Image processing and 3D movies were assembled by using Image-Pro 5.2 analyzer and 3D Constructor (Media Cybernetics, CA, USA). Data acquisition and processing was achieved with a Pentium IV PC (1.8 Ghz).

Image acquisition of 3D stacks. The piezoelectric device was excited with a 70 Hz triangular waveform via the piezoelectric device (PD) high current amplifier (Fig. 2). The camera acquired 60 images every 1/70 s, 30 for the positive ramp and 30 for the negative ramp (4200 images/s). This generates a *Z* resolution of 3.2 μm over a 100 μm depth and enables a higher sampling rate since 3D tracking information can be obtained from both up/down movement of the PD. This depth resolution is sufficient for an adequate 3D tracking of sperm, given that the mean length of their head is around 4 μm and that their *X*,*Y* displacement between stacks is around 3.3 μm for a mean speed of 200 μm/s. The alternative use of a ramp signal is not recommended since, while providing a higher *Z* resolution of 1.2 μm, the PD is forced into a faster return, compared to the smoothed return of the negative ramp of the triangular waveform. In fact, the PD, due to its own inertia (and that of the attached objective), is not able to follow the frequency components of a ramp signal at the used rate. A triangular waveform enables a smoother up/down movement of the PD. The PD was used in an open loop configuration without feedback from its servo-controller. This configuration permitted a larger *Z* displacement of 100 μm (about twice the depth if used in closed loop) while sacrificing the possibility of micro-positioning the PD to exact discrete points; nevertheless, the *Z* positions were obtained by linear interpolation after a calibration procedure described in System calibration. Sequences of 1.5 s (105 stacks) were recorded for each sampling condition using the camera's memory buffer and transferred via the USB-2 port to the computer as an .AVI compressed file.

System calibration. For *X*,*Y* calibration of the system the stage micrometer was immersed in the Petri dish filled with sea water to avoid calibration errors due to differential light refraction. An external *Z* calibration was also required since the PD was configured in open loop for a larger *Z* displacement. This was achieved by measuring the maximal displacement provided by the piezoelectric device when applying the triangular 70 Hz signal. First, with the PD off, a fixed circular object was focused at the center of the observation field. Then, turning on the PD, several image stacks were recorded at 4200 images per second (at this time, the focus of the microscope is moving according to the triangular signal provided). Each acquired stack contained a set of images of the fixed object while being maximally defocused when the sign of the slopes of the triangular signal changed from positive to negative and perfectly focused when passed from negative to positive

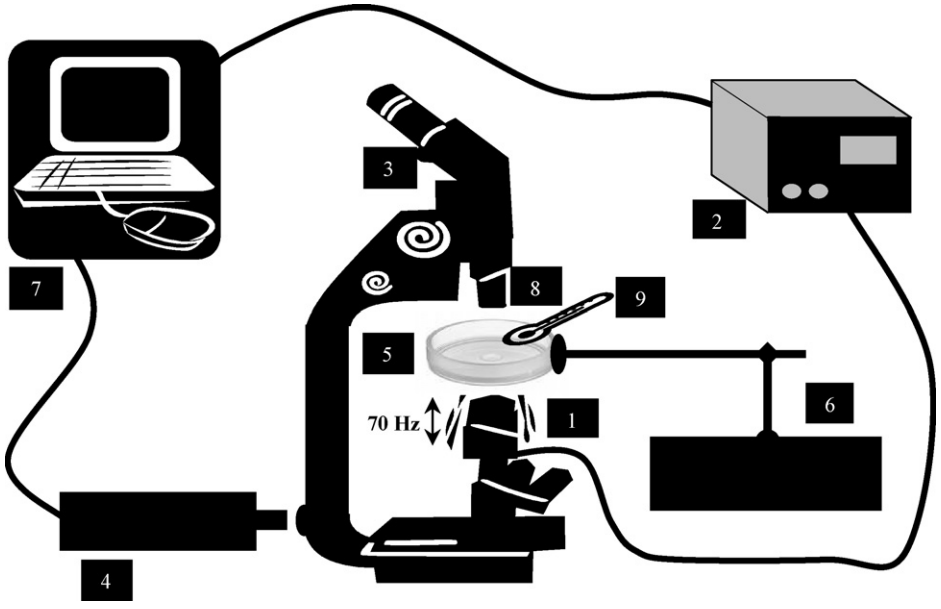

Fig. 1. Configuration of the 3D multi-sperm image acquisition system. (1) Piezoelectric device attached to the microscope long working distance objective; (2) Servo-controller; (3) Inverted microscope; (4) High speed video camera; (5) Imaging chamber; (6) Isolated support for imaging chamber; (7) Computer; (8) Condenser; (9) Thermocouple probe (+−0.1 °C).

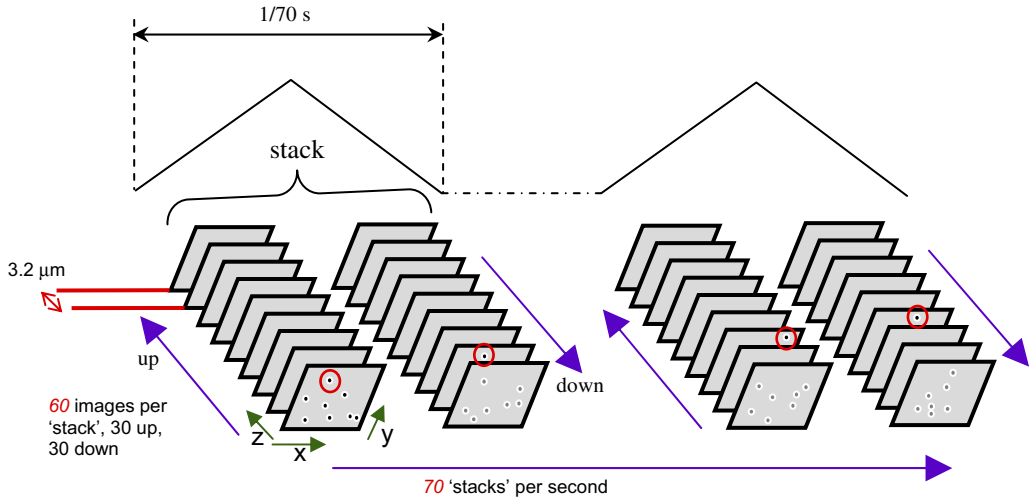

Fig. 2. High speed image stack acquisition for multi-sperm tracking. The circle surrounding the black point represents a single sperm moving over the 3D space of image stacks. At top, triangular signal feeding the PD.

(top and bottom of the triangular waveform). Then, a maximally defocused image of the circular object was located in the acquired movies (by measuring the lowest contrast feature with the image analyzer). This contrast feature was saved, then, with the PD off, the circular object was manually focused to the point of maximum contrast. Then, the micrometrical knob of the microscope (1 µm resolution graved scale) was turned manually to find exactly the same defocused image of the fixed object (by measuring the same contrast feature as that recorded previously), while deducing the final real displacement of the *Z* focal plane from the microscope's engraved focus wheel. This measured the largest *Z* displacement between acquired stacks which accurately provided the corresponding depth calibration. This procedure was repeated for each sample of experimental conditions.

3D tracking of spermatozoa. While multiple high-performance 3D tracking algorithms have already been published such as Genovesio et al., [15], under our experimental conditions, sperm trajectories were obtained manually as the main focus of the present work was the high speed acquisition of 3D data. By observing the first acquired stacks, a located sperm appearing when the microscope objective is moving in the upper direction (positive ramp of the triangular waveform), should appear again in a nearby position when the objective is moving down (negative ramp). Nevertheless, we have observed a constant *X*,*Y* shift between the position of the located sperm in the positive ramp and the negative one. This effect was due to a vibration artifact produced by the oscillation of the PD. While this vibration does not affect the Petri dish and the sperm preparation since it was mounted in a separated support (Fig. 1), it complicated the visual tracking of sperm. This artifact was eliminated subtracting the displacement of a fixed object in the sea water between successive image stacks from the sperm movies. Alternatively, since the introduced vibration has a constant phase with respect to the oscillation of the objective, we observed that spermatozoa appeared consecutively with no shift if tracked only in the 'positive' stacks or only in the 'negative' ones. Our group is currently working to avoid this mechanical artifact, however in this work the tracking procedure was performed only in positive ramps (30 images per ramp), loosing half of the temporal resolution but retaining enough to reconstruct sperm trajectories from the stacks as mentioned in Image acquisition of 3D stacks.

Manual tracking was performed as follows: The first 30 image half-stack (corresponding to the first positive ramp) was scanned to find 'in focus' sperm which were tagged. The same sperm were located in the following stack (displacing the image counter by 60 images) and searching in adjacent images. Since the *X*,*Y*,*Z* displacement of the sperm was small between stacks, it was possible to locate visually the same tagged spermatozoa within subsequent stacks. The 3D coordinates of tracked sperm were then recorded. For the three sea urchins from which sperm samples were collected, a total of 262 spermatozoa were recorded. Of these, 21% provided useful data, as of the rest, 13% were stationary, 27% did not remain in the analyzed volume for the required time of 1 s and 40% were excluded due to the presence of other nearby spermatozoa. Further development of automated video tracking procedures in our group is underway to improve these limitations.

Speed and radius of curvature estimation. The mean speed of each sperm was calculated by averaging the magnitude of each consecutive vector of linear velocity between two adjacent trajectory points. The radius of curvature was calculated using a Hough transform (HT) based method [16]. The HT is a mathematical technique for detecting specific shapes (as circles) by mapping actual points from the real space (in our case consecutive points of a sperm trajectory) to features over a parameter space (for example, the radius of a circle passing through sets of three consecutive non-collinear points along the trajectory that describe the helix [7]). Each extracted feature votes for the circle that could pass through it. The votes are collected in an accumulation array where its maxima correspond to the center (x_i, y_i, z_i) of circumference of radius r_i. Peaks in the Hough space correspond to the more representative radius along the trajectory. These radii are averaged to obtain the estimated equivalent radius of curvature of the whole trajectory.

Results

Fig. 3 shows the helical trajectory of single tracked spermatozoa swimming freely for a period of 1 s in 3D (Fig. 3a and c) and 2D (Fig. 3b and d). Fig. 4 illustrates two real 3D reconstructed scenes (free-swimmers and surface-confined sperm swimming in 2D) with several sea urchin sperm tracked in a sea water volume in a Petri dish, both for a period of 1 s. These videos can be visualized as Supplementary material in the on-line publication as well as in our Web site [17].

We have analyzed the speed and radius of curvature of two groups of 27 spermatozoa, one group for 2D confined sperm and another for free swimmers (Table 1). Data were obtained from three different sea urchins, nine spermatozoa from each urchin swimming in the same volume at the same time. The first group swam near the flat surface of the imaging chamber (describing cir-

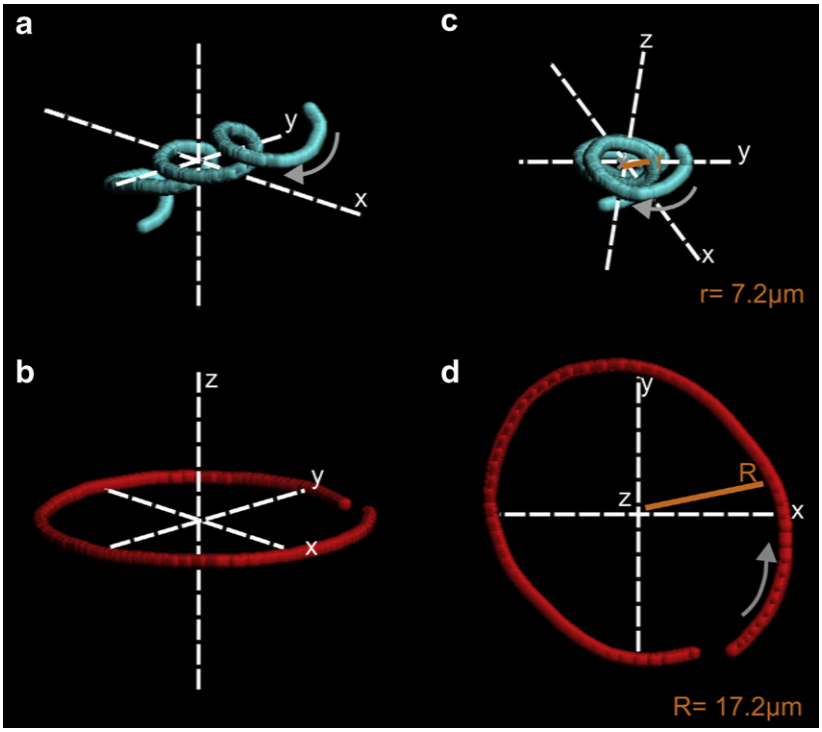

Fig. 3. Trajectory of tracked sea urchin spermatozoa swimming during 1 s. (a) Free swimmer, (b) 2D surface-confined, (c) Free swimmer upper view (from helical axis), (d) 2D confined upper view to compare diameters.

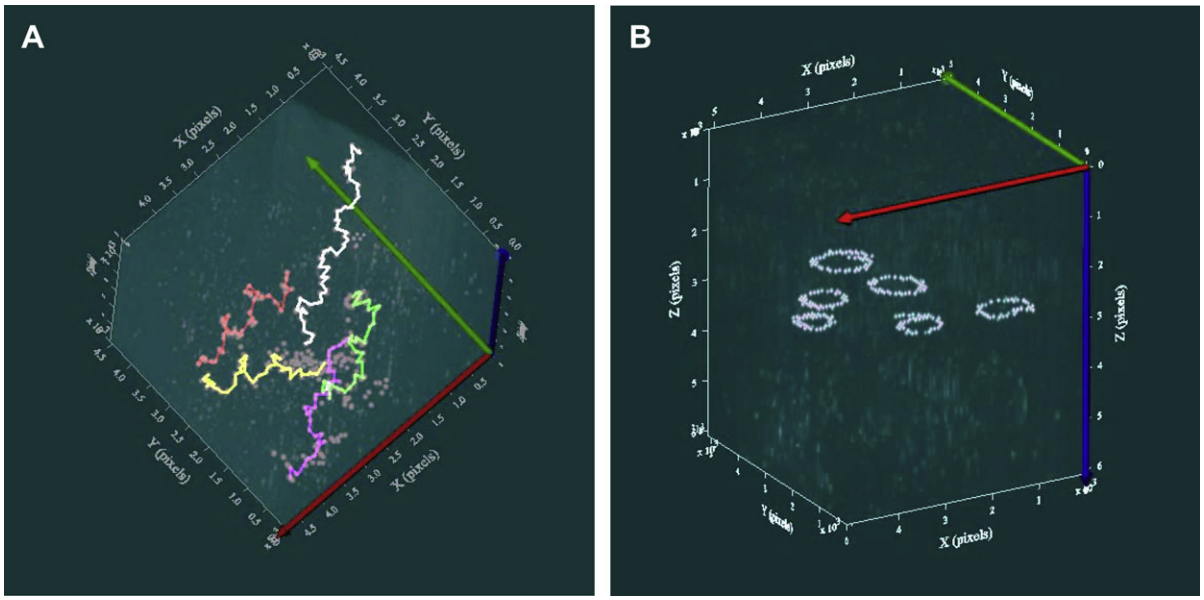

Fig. 4. Real reconstructed 3D scenes showing the trajectory of multiple tracked spermatozoa for a period of 1 s, (Pixels 10×, 1 pixel = 2.33 μm). (A) Free-swimmers, (B) Swimming sperm confined in 2D. Sperm trajectories are colored for ease of discrimination. Supplementary video material is available in the online publication as well as in our Web site [17].

Table 1
Speed, radius of curvature and revolutions/s comparison for 2D surface-confined vs 3D free-swimming sperm

Sea urchin	Mean speed (μm/s)		Mean radius of curvature (μm)		Circular revolutions/s	
	2D swim	3D free swim	2D swim	3D free swim	2D swim	3D free swim
1	132 ± 6.3	167 ± 5.7	16.5 ± 0.7	7.5 ± 1.15	1.3 ± 0.17	4.3 ± 0.6
2	145 ± 7.04	189 ± 7.54	16 ± 1.85	6.5 ± 0.65	1.3 ± 0.19	4.3 ± 0.74
3	127 ± 7.9	183 ± 4.7	15.5 ± 1.85	6.5 ± 1.45	1.3 ± 0.16	3.4 ± 0.88

cular trajectories), while the second group swam freely in the sea water volume (describing helical pathways). The surface-confined group swam 25% ($\alpha < 0.05$) slower than the free-swimming group (one-factor ANOVA). Moreover, the average number of complete circular revolutions for the first group (1 revolution/s) was 3-fold fewer than the free-swimming sperm, while their mean radius of curvature was 134% greater.

Discussion and conclusions

Though motility is fundamental for fertilization and the most easily observed sperm function, it is only partially understood. We have presented a novel method for acquiring three-dimensional information for multiple free-swimming sperm simultaneously during 1 s. By measuring simple parameters such as mean speed and number of completed circular revolutions in two different sperm groups, we show that the proximity to a nearby surface impacts the motile behavior of sea urchin sperm. This may have important implications for currently published analyses of sperm swimming parameters and their dynamic regulation during processes such as chemotaxis, which have been nearly universally obtained with sperm swimming in 2D (e.g. [18]). Such studies must be viewed with precaution given our current results which show that sperm trajectories in (more physiologically relevant) 3D are significantly at variance with those of swimming sperm confined in 2D. Further studies are ongoing to better characterize these changes.

The structure of the axoneme, the propulsion machinery of cilia and flagella, is conserved throughout eukaryotes, albeit with rare exceptions [19,20]. Furthermore, most cells in our body possess cilia which play important roles in reproduction, development, sensing, and other functions. Cilia defects can cause infertility, developmental problems, cystic fibrosis, obesity, and diabetes [21]. The tools developed to study the 3D swimming behavior of sea urchin sperm will therefore have an impact on our understanding on how cilia and flagella regulate their movement and transduce information.

Acknowledgments

We acknowledge the financial support of UNAM (DGAPA Grants IN104207-2 to GC and IN-225406 to AD), and The Wellcome Trust and CONACyT (24974) to AD. The authors thank Juan Manuel Hurtado for computer support and S. Ainsworth for bibliographic assistance.

Appendix A. Supplementary data

Supplementary data associated with this article can be found, in the online version, at doi:10.1016/j.bbrc.2008.05.189.

References

[1] J.M. Nascimento, L.Z. Shi, S. Meyers, P. Gagneux, N.M. Loskutoff, E.L. Botvinick, M.W. Berns, The use of optical tweezers to study sperm competition and motility in primates, J. R. Soc. Interface 5 (2008) 297–302.
[2] R. Miller, Sperm chemo-orientation in the metazoan, in: C. Metz, A. Monroy (Eds.), Biology of Fertilization, Academic Press, New York, 1985, pp. 275–337.
[3] H.S. Jennings, On the significance of the spiral swimming of organisms, Am. Nat. 35 (1901) 369–378.
[4] Y. Hiramoto, S.A. Baba, A quantitative analysis of flagellar movement in echinoderm spermatozoa, J. Exp. Biol. 76 (2002) 85–104. 1978.
[5] H.C. Crenshaw, Helical orientation: a novel mechanism for the orientation of microoganisms, Lect. Notes Biomath. 89 (1990) 361–386.
[6] H.C. Berg, The tracking microscope, Adv. Opt. Electron Microsc. 7 (1978) 1–15.
[7] H.C. Crenshaw, Analysis of three-dimensional trajectories of organisms: estimates of velocity, curvature and torsion from positional information, J. Exp. Biol. 203 (2000) 961–982.
[8] H.C. Crenshaw, Orientation by helical motion-I. Kinematics of the helical motion of organisms with up to six degrees of freedom, Bull. Math. Biol. 55 (1) (1993) 197–212.
[9] H.C. Crenshaw, Orientation by helical motion-II. Changing the direction of the axis of motion, Bull. Math. Biol. 55 (1) (1993) 213–230.
[10] H.C. Crenshaw, Orientation by helical motion-III. Microorganisms can orient to stimuli by changing the direction of their rotational velocity, Bull. Math. Biol. 55:1 (1993) 231–255.
[11] H.C. Crenshaw, A new look at locomotion in microorganisms: rotating and translating, Am. Zool. 36 (1996) 608–618.
[12] H.C. Crenshaw, C.N. Cianpaglio, M. McHenry, Analysis of the three-dimensional trajectories of organisms: estimates of velocity, curvature and torsion from positional information, J. Exp. Biol. 203 (2000) 961–982.
[13] B.M. Friedrich, F. Jülicher, Chemotaxis of sperm cells, PNAS 104 (33) (2007) 13256–13261.
[14] J. Cosson, P. Huitorel, C. Gagnon, How sperm come to be confined to surfaces, Cell Motil. Cytoskeleton 54 (2003) 56–63.
[15] A. Genovesio, T. Liedl, V. Emiliani, W.J. Parak, M. Coppey-Moisan, J.C. Olivo-Marin, Multiple particle tracking in 3-D+t microscopy: method and application to the tracking of endocytosed quantum dots, IEEE Trans. Image Process. 15 (5) (2006) 1062–1070.
[16] P.V.C. Hough, Methods and means for recognizing complex patterns, US Patent (1962) 3,069,654.
[17] WEB site of the Image Analysis and Computer Vision Laboratory of the Instituto de Biotecnología, UNAM: http://www.ibt.unam.mx/labimage.
[18] C.D. Wood, T. Nishigaki, Y. Tatsu, N. Yumoto, S.A. Baba, M. Whitaker, A. Darszon, Altering the speract-induced ion permeability changes that generate flagellar Ca^{2+} spikes regulates their kinetics and sea urchin sperm motility, Dev. Biol. 306 (2007) 525–537.
[19] B. Baccetti, Evolutionary trends in sperm structure, Comp. Biochem. Physiol. A. 85 (1986) 29–36.
[20] D. Mitchell, Speculations on the evolution of 9+2 organelles and the role of central pair microtubules, Biol. Cell 96 (2004) 691–696.
[21] W. Marshall, The cell biological basis of ciliary disease, J. Cell Biol. 180 (2008) 17–21.